Materials and Design 99 (2016) 273–283

Contents lists available at ScienceDirect

Materials and Design

journal homepage: www.elsevier.com/locate/matdes

Mitigating distortion and residual stress by static thermal tensioning to improve fatigue crack growth performance of MIG AA5083 welds

M.N. Ilman [a,*], Kusmono [a], M.R. Muslih [b], N. Subeki [a], H. Wibowo [a]

[a] Department of Mechanical and Industrial Engineering, Gadjah Mada University, Yogyakarta, Indonesia
[b] National Nuclear Energy Agency of Indonesia (BATAN), Serpong, Banten, Indonesia

ARTICLE INFO

Article history:
Received 11 November 2015
Received in revised form 25 February 2016
Accepted 9 March 2016
Available online 15 March 2016

Keywords:
Out of plane distortion
Residual stress
Fatigue
Static thermal tensioning

ABSTRACT

The demand for lightweight structures in ship fabrication to improve performance and fuel savings has led to increasing use of thin-section structures. However, welding such structures often produces problems such as distortion and residual stress. The present investigation is aimed to mitigate distortion and residual stress using static thermal tensioning (STT) to improve fatigue performance in AA 5083 metal inert gas (MIG) welded joints. The STT treatments were performed by cooling the weld zone and its adjacent area during welding whereas both sides away from the weld were heated at various temperatures of 100, 200 and 300 °C to generate thermal gradient. Subsequent experiments including distortion measurements, microscopical examination, hardness and tensile tests, measurements of residual stresses using neutron diffraction method and fatigue crack growth tests combined with SEM fractography were conducted. Results showed that an increase in heating temperature reduced convex longitudinal out of plane distortion. The minimum longitudinal out of plane distortion was achieved at a heating temperature of 200 °C owing to the balance between buckling distortion induced by welding and that generated by static differential heating which opposed the weld distortion. Under such condition, fatigue crack growth performance was improved.

© 2016 Elsevier Ltd. All rights reserved.

1. Introduction

Aluminium-magnesium alloys designated as 5xxx series alloys have been widely used in marine applications such as ship structure and superstructure of ocean-going vessels due to their lower weight, relatively high strength and excellent corrosion resistance. One of these alloys is AA5083 that is Al-4.5%Mg-1%Mn alloy where its strength is resulted from solid solution strengthening due to magnesium additions and strain hardening [1]. Moreover, this alloy is considered to have good weldability since it has hot cracking resistance and meets required mechanical strength at the weld joint [2].

Welding is one of the most critical manufacturing processes in modern ship fabrication since a ship construction today consists of many structural elements that are welded during assembly. Among fusion welding processes, a metal inert gas (MIG) welding is the most common joining process for aluminium alloys [3]. To date, a trend in design and manufacturing practice is to use thin-plate structures to reduce product weight but welding such structures tends to increase distortion and residual stress. Buckling distortion often referred to out of plane distortion causes some problems, i.e. it reduces dimensional accuracy, it can cause loss of structural integrity and it increases manufacturing cost due to additional correction works [4].

A number of works has been carried out to study weld distortion and residual stress. It is known that weld heat flow studies which were initially treated using analytical approach [5–7] have become increasingly important as basic principles for understanding weld distortion and residual stress. Recently, the increase in computational power has enabled researchers [8–13] to apply finite element (FE) model to gain better quantitative understanding of distortion and residual stress which are important to develop distortion-controlled methods [14–15]. A particular attention is paid to in-process methods since they have advantages over conventional post weld correction techniques, i.e. the elimination of distortion takes place prior to and during welding process hence avoiding costly reworking operation after welding [16]. Currently, thermal-based in-process control methods which employ additional heating with and without cooling sources during welding are more desirable than those based on mechanical techniques. This is because thermal stretching generated by differential heating is more efficient compared to mechanical stretching which requires complex setup and large forces for large structures.

The application of thermal effect for mitigating weld distortion and residual stress prior to and during welding was first reported by Burak et al. [17,18] who developed thermal tensioning method, often known as static thermal tensioning (STT). This technique involves resistive heating bands located at both sides away from the weld whereas the weld zone is quenched simultaneously. The effectiveness of static thermal tensioning has been evaluated by Michaleris and Sun [19] using

* Corresponding author.
E-mail address: ilman_noer@ugm.ac.id (M.N. Ilman).

http://dx.doi.org/10.1016/j.matdes.2016.03.049
0264-1275/© 2016 Elsevier Ltd. All rights reserved.

finite element analysis. According to the authors, thermal tensioning technique is able to reduce residual stress below the critical buckling level hence avoiding structural buckling. Consistent with this finding, Guo and Li [20] have reported that STT reduces longitudinal plastic compression in the weld resulting in lower distortion and residual stress.

Another approach known as transient thermal tensioning (TTT) has also been developed as an alternative distortion control technique [21–23]. Unlike STT, the TTT technique employs movingly localised heating sources to generate tensioning stresses without quenching. Furthermore, Guan [24] has categorised effects of thermal tensioning into two different types, namely the overall cross-section thermal tensioning and the localised thermal tensioning. In the former, the thermal tensioning which consists of preset cooling and heating is applied along the cross section of welded plates. This method is the modification of STT technique by employing 'two-point' finger clamping system termed as Low Stress No Distortion (LSND) whereas the latter is carried out by locating a cooling source following the moving weld torch to locally cool the weld. This new developed technique is known as Dynamically Controlled Low Stress No Distortion (DC-LSND). Recent investigations conducted numerically and experimentally have shown that DC-LSND is proved to be effective for control of distortion and residual stress [25–26].

In modern engineering practice, welded structures are often subjected to dynamic or fluctuating loads during service. Under such condition, the presence of tensile residual stress in the welded joints can promote fatigue failure at a stress below its static strength [27–29]. Current researches on thermal tensioning are mostly focused on mitigation of distortion and residual stress and there have been limited data on how these techniques, in particular static thermal tensioning (STT) to affect mechanical properties and fatigue performance of the welded structures. Therefore, it is the subject of the present investigation.

2. Experimental procedures

2.1. Welding conditions

In order to obtain experimental data with greater consistency, an automatic MIG welding equipment was employed in this investigation. The materials used were aluminium alloy AA5083 plates welded using a filler metal of ER5356 and their chemical compositions are given in Table 1. Two AA5083 plates having dimension of 400 mm × 100 mm × 3 mm were butt welded along 400 mm. The plates were clamped using simple supports as reported by Gray et al. [13]. Details of the filler material data and welding parameters used are given in Table 2.

The STT treatments were carried out by locating a cooling system underneath the weld zone and simultaneously, both regions away from the weld zone were heated using resistive heating bands at various temperatures of 100, 200 and 300 °C to generate thermal gradient as shown in Fig. 1. The cooling system was made of copper backing bars having drilled water passages to provide quenching. Three thermocouples, designated as TC1, TC2 and TC3 were attached to the welded plates at the distances of 10, 20 and 30 mm respectively from the weld centreline to monitor temperatures during welding. The STT-free welded plate specimens (as welded condition) and the specimens with quenching only were also produced for the reference welds.

Of note is that the cooling intensity should be carefully controlled to reduce out of plane distortion and residual stress effectively. Therefore, it is necessary to analyse heat energy source, heat loss and heat sink. In the case of welding with quenching only (heat sink welding), the heat energy transferred from the heat source to the cooling system as shown in Fig. 1 could be analysed as follows. Due to heat losses, the net heat energy (Q_{net}) during welding is given by:

$$Q_{net} = \eta Q_{in} = \eta EI \tag{1}$$

where Q_{in} is heat generated by welding (Watt), η is heat transfer efficiency, E is welding voltage (V) and I is welding current (A). A portion of the net heat energy is transferred to heat sink (Q_s) and the remaining heat energy (Q_r) is lost to the surroundings so that:

$$Q_{net} = Q_s + Q_r. \tag{2}$$

The heat transferred to heat sink is given by:

$$Q_s t_{weld} = \int_0^{\infty} mc[T_{out}(t)\text{-}T_{in}]dt \tag{3}$$

where m is mass flow rate of water (g/s), c is specific heat of water (J/(g.°C)), T_{in} is inlet water temperature (°C), T_{out} (t) is temperature of water leaving the copper baking bars which varies with time (°C) and t_{weld} is welding time (s). If the net heat energy (Q_{net}) is transferred completely to heat sink then the energy balance is given by:

$$Q_{net} t_{weld} = \eta EI t_{weld} = \int_0^{\infty} mc[T_{out}(t)\text{-}T_{in}]dt. \tag{4}$$

Referring to Eqs. (3) and (4), the cooling intensity could be determined by controlling mass flow rate and temperature of cooling water.

2.2. Distortion and residual stress measurements

The longitudinal out of plane distortions (displacement in Z-direction) in Fig. 2 were measured at the edge of the welded plates along a longitudinal direction (X-direction) using dial indicators.

Longitudinal and transverse residual stresses were measured using neutron diffraction technique at middle part of the welded plate length. The measurements were taken along transverse distance, starting from the weld centreline to the edge of the welded plate as indicated by the plane A-B in Fig. 2. The neutron beam with the wave length of 1.83375 Å was diffracted on (311) reflection at the diffraction angle (2θ) of 96.5°. Lattice parameters were measured in the x (longitudinal), y (transverse) and z (through-thickness) directions using a gauge

Table 2
Materials and welding parameters.

Filler material	:	ER5356
Wire diameter	:	0.8 mm
Wire speed	:	9 m/min.(150 mm/s)
Shielding gas	:	Argon (Ar)
Gas flow	:	14 l/min
Voltage	:	20 Volt
Current	:	100 A
Welding speed	:	10 mm/s
Water flow	:	1200 l/h

Table 1
Chemical compositions of AA 5083 plates and ER 5356 filler metals (wt%).

Material	Mg	Mn	Si	Fe	Cr	Cu	Zn	Ti	Al
AA 5083	4.5	0.65	0.26	0.22	0.09	0.09	0.06	0.03	Bal.
ER 5356	4.5–5.5	0.05–0.20	0.25	0.40	0.05–0.20	0.10	0.10	0.06–0.20	Bal.

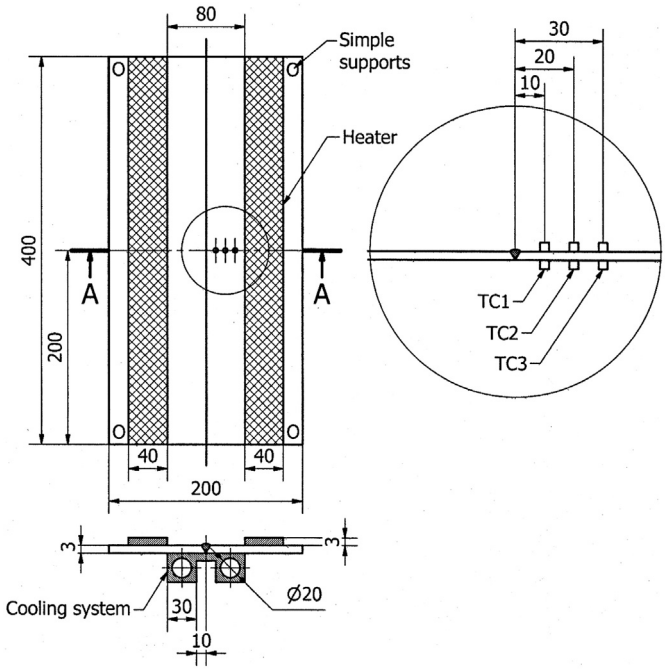

Fig. 1. Experimental setup for a MIG-welding process with STT treatment facilities.

volume of 8 mm^3 having dimension of 2 × 2 × 2 mm^3. This gauge volume size, i.e. 8 mm^3 was considered to be the minimum volume size which contained a number of grains statistically accepted for sampling to give representative data as reported by Webster and Wimpory [30]. Since the widths of weld metal and HAZ regions in the welded plates under study were relatively large, typically more than 2 mm, even for narrow HAZ region then variation in the weld microstructures can be measured using this volume size with no interference from other different microstructures. The residual strains were calculated as follow:

$$\varepsilon_{hkl} = \frac{d_{hkl} - d_o}{d_o} \tag{5}$$

where d_{hkl} and d_o are stressed and stress-free lattice parameters respectively. The stress-free lattice (d_o) was measured from a small section with dimension of 10 mm × 5 mm × 3 mm cut off from the side of the welded plate specimen to provide the released residual stress. The strains (ε_{ii}) measured in triaxial principal directions, $i = x,y,z$ can be used to calculate residual stresses (σ_{ii}) using Hooke's law as given in Eq.(6).

$$\sigma_{ii} = \frac{E}{1+\nu}\varepsilon_{ii} + \frac{\nu E}{(1+\nu)(1-2\nu)}\Sigma\varepsilon_{ij}. \tag{6}$$

In the case of a thin plate loaded in the plane of the plate with no stress normal to a free surface, i.e. $\sigma_{zz} = 0$, plane stress condition exists so that the longitudinal (σ_{xx}) and transverse (σ_{yy}) residual stresses can be calculated according to:

$$\sigma_{xx} = \frac{E}{1-\nu^2}\left(\varepsilon_{xx} + \nu\varepsilon_{yy}\right) \tag{7}$$

$$\sigma_{yy} = \frac{E}{1-\nu^2}\left(\varepsilon_{yy} + \nu\varepsilon_{xx}\right). \tag{8}$$

The macroscopic values of Young's modulus (E) and Poisson's ratio (ν) for aluminium alloys were taken 70 GPa and 0.3 respectively.

2.3. Microstructural examination

Optical micrographs were taken from cross section of the welds. The samples were prepared according to a standard metallography technique with etchant used was Keller reagent (2 ml HF + 3 ml HCl + 5 ml HNO_3 + 190 ml H_2O).

2.4. Mechanical tests

Tensile tests were carried out using transverse weld specimens according to ASTM E8M whereas hardness distributions along weld metal, HAZ region and base metal were measured using Vickers microhardness with the load of 100 grf.

2.5. Fatigue crack growth tests and SEM fractography

The fatigue crack growth (FCG) tests were conducted using a servo-hydraulic machine. Centre-cracked tension (CCT) specimens were prepared according to ASTM E647. Each specimen had the initial crack located at the weld region as shown in Fig. 3. The FCG tests were conducted under sinusoidal load having a constant amplitude load whereas the stress ratio (R) and frequency (f) used were 0.1 and 11 Hz respectively. Subsequently, the fracture surfaces were examined using SEM at the stable crack growth region or region II of da/dN-ΔK curves.

3. Results and discussion

3.1. Weld thermal cycles

The thermal cycles of each welded plate specimen were studied by locating three thermocouples, namely TC1, TC2 and TC3 at the distances of 10, 20 and 30 mm respectively away from the weld centreline. Referring to Fig. 4a, it can be seen that each thermal cycle in a conventional welding was marked by a rapid increase in temperature as a welding torch moved to a thermocouple until a peak temperature was achieved followed by a relatively slow temperature decrease as the torch passed the thermocouple. It can be seen that an increase in distance to the weld line reduced the peak temperature. These results seem to be consistent with a classical Rosenthal analytical solution of temperature field [5,7,31] for thin plates as given by:

$$T - T_o = \frac{q_w}{h(4\pi k\rho ct)^{1/2}}\exp\left(-\frac{r^2}{4\alpha t}\right) \tag{9}$$

where q_w is heat input defined as (Q/v), Q is heat energy, v is travelling speed, T_o is initial temperature, k is thermal conductivity, (ρc) is specific

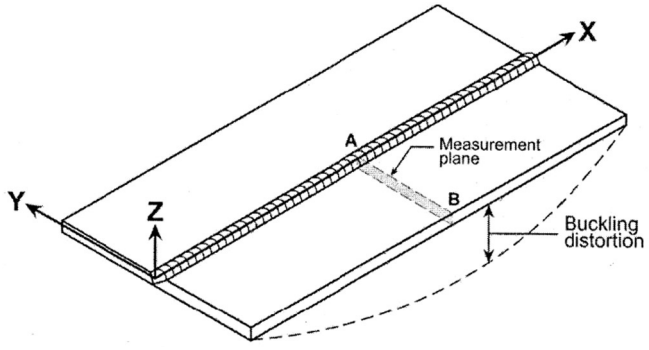

Fig. 2. Distortion and residual stress measurements.

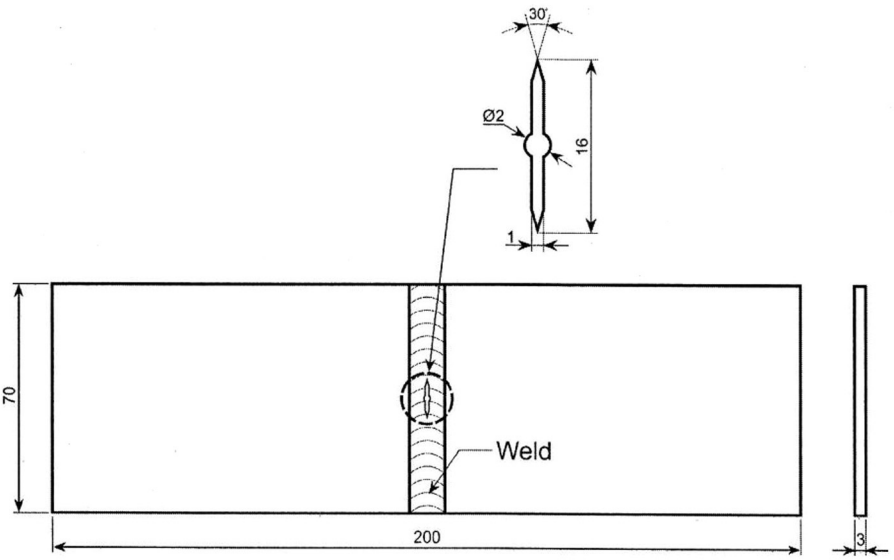

Fig. 3. Centre-cracked tension (CCT) specimen.

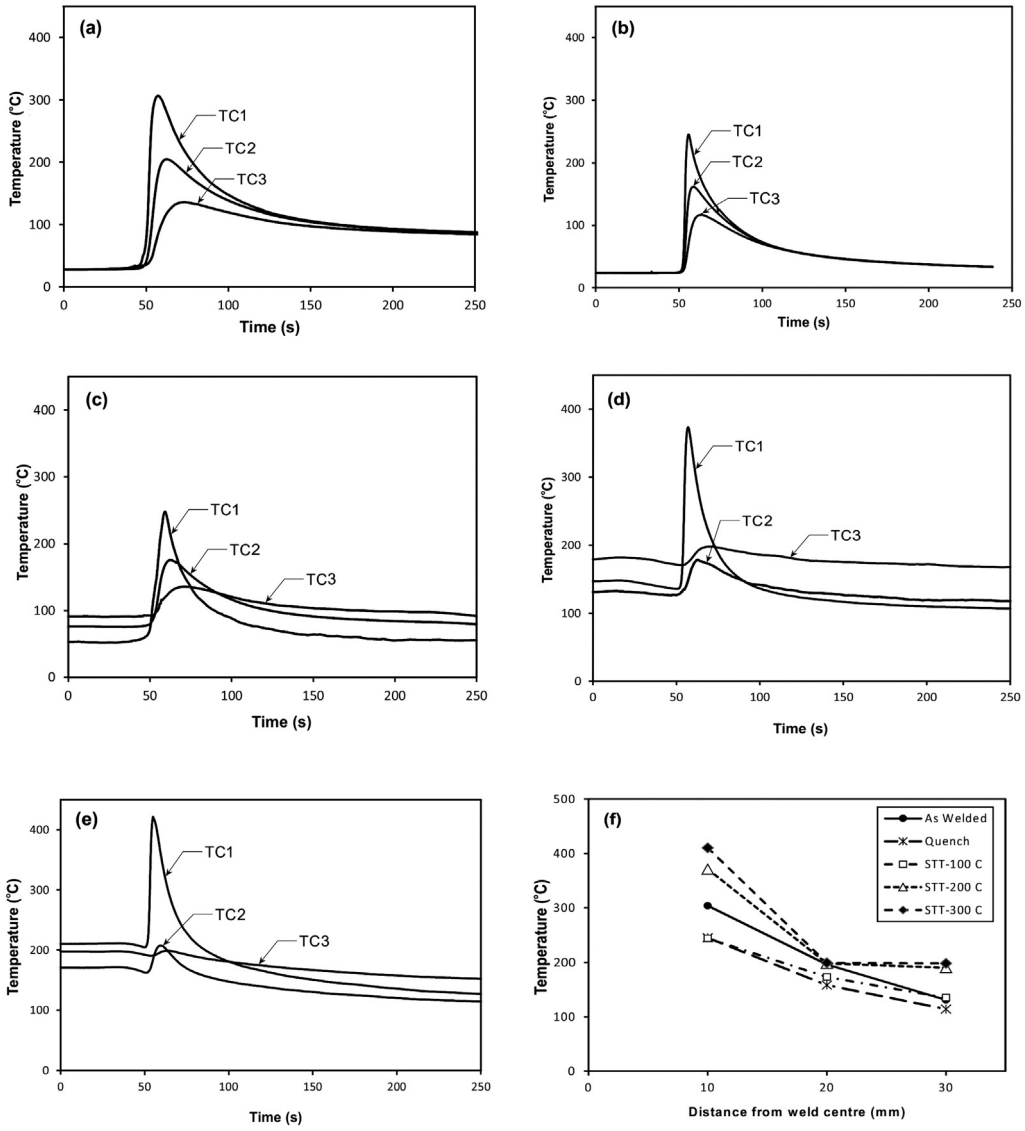

Fig. 4. Weld thermal cycles in: (a) as welded, (b) quenching only, (c), (d), (e) STT-treated conditions with heating temperatures of: 100 °C, 200 °C, 300 °C respectively and (f) peak temperature distributions between weld zone and electric heating band for all welds.

heat per unit volume, α is thermal diffusivity defined as $k/(\rho c)$, h is plate thickness, t is time and r is radial/lateral distance from the weld.

Effect of STT treatment can be seen from the weld thermal cycles in Fig. 4. It seems that the use of cooling or quenching at the weld region and additional heating sources away from the weld region modifies the weld thermal cycles and temperature fields. The peak temperatures recorded by TC1, TC2 and TC3 in the welded plate under quenching only (Fig. 4b) are lower than the as welded condition (Fig. 4a). Subsequently, combined effect of quenching and heating produces STT treatments as shown in Fig. 4c–e. The peak temperatures of the STT-treated weld increase as the heating temperature is increased up to100 °C (Fig. 4c) but they are still lower than those observed in the as welded condition (Fig. 4a). It seems that the additional heating is not sufficient to contribute temperature increase in the region near the weld zone due to quenching from the cooling system. However, reversal effect is observed as the heating temperature is further increased to 200 °C (Fig. 4d) or 300 °C (Fig. 4e) marked by their higher peak temperatures. These higher heating temperatures are expected to increase thermal tensioning effect.

The peak temperature distributions at the region between weld zone and heating bands for all weld specimens under study are shown in Fig. 4f. In comparison with as welded condition, the weld specimen under quenching only has lower peak temperatures at the distance of 20 mm (or more) from the weld centreline whereas the peak temperatures of both weld specimens start to coincide at the closer distance, typically 10 mm from the weld centreline. This suggests that quenching only can reduce the peak temperatures in the vicinity of the weld zone but it has no significant effect on the peak temperature of fusion or weld zone. As the result, the region near the weld zone has relatively steep gradient temperature due to quenching. On the other hand, the STT treatments seem to increase the peak temperatures at the distance of 10 mm from the weld centreline with 'kinks' are observed the distance of 20 mm, especially for heating temperatures of 200 and 300 °C. Such temperature profiles also produce steep temperature gradients at the regions near the weld zone.

3.2. Longitudinal out of plane distortions

Fig. 5 shows out of plane distortions in the welded plates prepared using the conventional welding process and the STT method. It can be seen that a low or almost no distortion is observed when the heating temperature of STT achieves 200 °C. For quantitative analysis, out of plane distortions along the longitudinal direction were measured for all welded plate specimens under investigation as shown in Fig. 6. Referring to Fig. 6, it can be seen that the conventional MIG welding process produces high convex longitudinal out of plane distortion with the maximum distortion is around 12 mm at the middle part of the welded plate

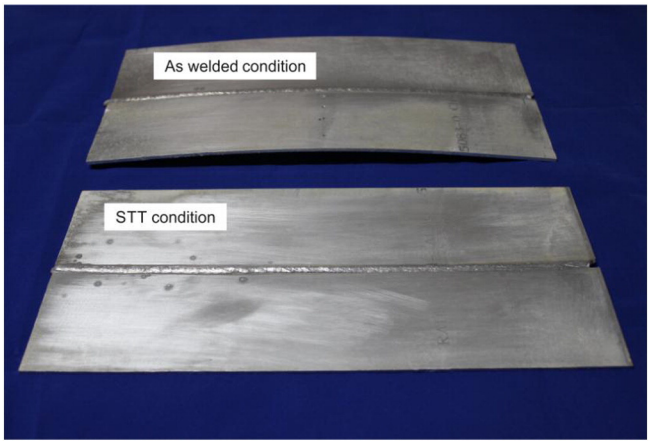

Fig. 5. Comparison of AA5083 plates welded by conventional welding and STT method.

length. The use of quenching only during welding reduces the out of plane distortion. The beneficial effect of quenching could be associated with a decrease in the peak temperature around the weld zone. Based on this finding, it can be predicted that further increase in cooling intensity would produce lower distortion in a similar manner to heat sink welding [25,32]. Unlike heat sink process which relies on quenching only, the STT treatment uses combined effect of quenching and additional heating during welding to reduce distortion. As the STT-treated welded plate is heated at100 °C, the distortion decreases and the optimum heating temperature is achieved at 200 °C. However, further increase in the heating temperature around 300 °C changes the direction of bowing resulting in concave out of plane distortion. These results seem to suggest that combined effect of quenching and heating is effective to mitigate distortion.

The mechanism of buckling distortion formation could be explained using analytical approach as shown in Fig. 7. This analysis is based on shrinkage forces (or shrinkage displacement) as the welding process goes to completion as suggested by Radaj [7].

As a heat source moves along a weld line with heat input of q_w, the temperature distribution around the weld follows Rosenthal's equation and the mean temperature increase, ΔT_o in the welded plate having dimension of h x w x l is given by:

$$\Delta T_o = \mu_l \frac{q_w}{\rho c A} \tag{10}$$

where μ_l is longitudinal stiffness factor, ρ is density, c is specific heat capacity and A is cross section area that is equal to w x h. The longitudinal shrinkage Δl of the plate with centric longitudinal weld is given by:

$$\Delta l = \alpha_T l \Delta T_o = \mu_l \frac{\alpha_T q_w l}{\rho c A} \tag{11}$$

where α_T is thermal expansion coefficient. The compressive longitudinal shrinkage stress (σ_s) can be calculated as follows:

$$\sigma_s = \varepsilon E = \frac{\Delta l}{l} E = \mu_l \frac{\alpha_T q_w E}{\rho c A}. \tag{12}$$

According to theory of simply supported rectangular plate, the critical buckling stress (σ_{cr}) is determined by [7,33]:

$$\sigma_{cr} = \frac{k\pi^2 E}{12(1-\nu^2)(w/h)^2} \tag{13}$$

where k is constant. Buckling distortion will occur if compressive longitudinal shrinkage stress (σ_s) which acts on the welded plate exceeds its critical buckling stress, σ_{cr}. Since aluminium alloys have relatively higher values of α_T, typically in the range of 2.3–2.7 $\times 10^{-5}$ K^{-1} and lower averaged ρc (2.7×10^{-3} J/mm^3 K) compared to other metals such as carbon steels, austenitic stainless steels and titanium alloys then based on Eq. (12), aluminium alloys are more susceptible to distortion.

In the welds treated by STT method, the buckling distortion is relatively low. It seems that introducing additional or secondary heating sources at both sides of a weld region and, simultaneously cooling at the weld region can generate static thermal tensioning which opposes buckling distortion. In conventional welding, buckling distortion occurs in a welded plate if compressive shrinkage stress (σ_s) is higher than its critical buckling distortion (σ_{cr}). In the case of STT condition, the formation of static thermal tensioning stress ($+\sigma_T$) due to preset temperature distribution opposes compressive shrinkage stress ($-\sigma_s$) resulting in $-(\sigma_s - \sigma_T)$ and the minimum distortion is achieved as the resultant stress $-(\sigma_s - \sigma_T)$ is close to zero. However, as the magnitude of σ_T is greater than σ_s then the value of $-(\sigma_s - \sigma_T)$ becomes positive and this probably changes the direction of buckling distortion.

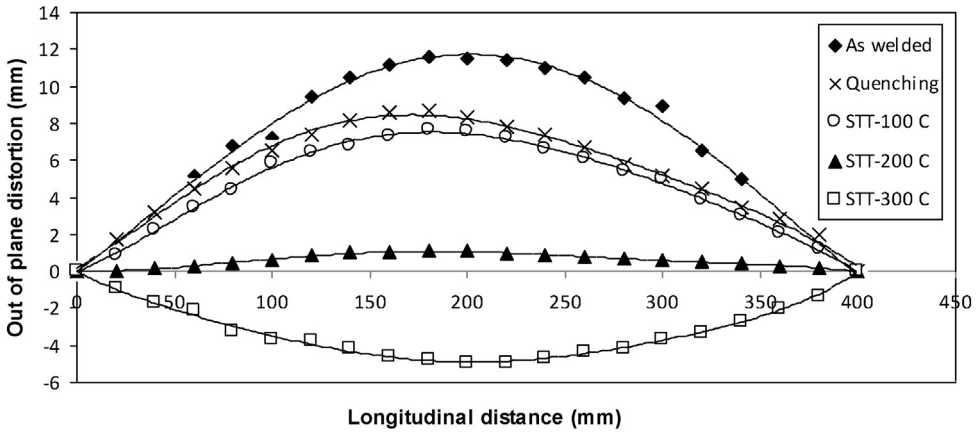

Fig. 6. Out of plane distortions of the welded plates under study.

The formation of thermal tensioning stress could be linked to temperature gradient as reported by a number of researchers [24,34]. In the case of STT welding, the localised secondary heating sources produce compressive stress during welding ($-\sigma_x$) where its magnitude is proportional to the temperature gradient ($\partial T/\partial y$). Subsequently, the compressive stress would induce the thermal tensioning stress ($+\sigma_T$) at the weld bead ($y=0$) due to static equilibrium condition. This leads to suggestion that an increase in the heating temperature at a distance y from the weld zone produces steep thermal gradients at both heating area and region around the weld zone hence increasing thermal tensioning effect.

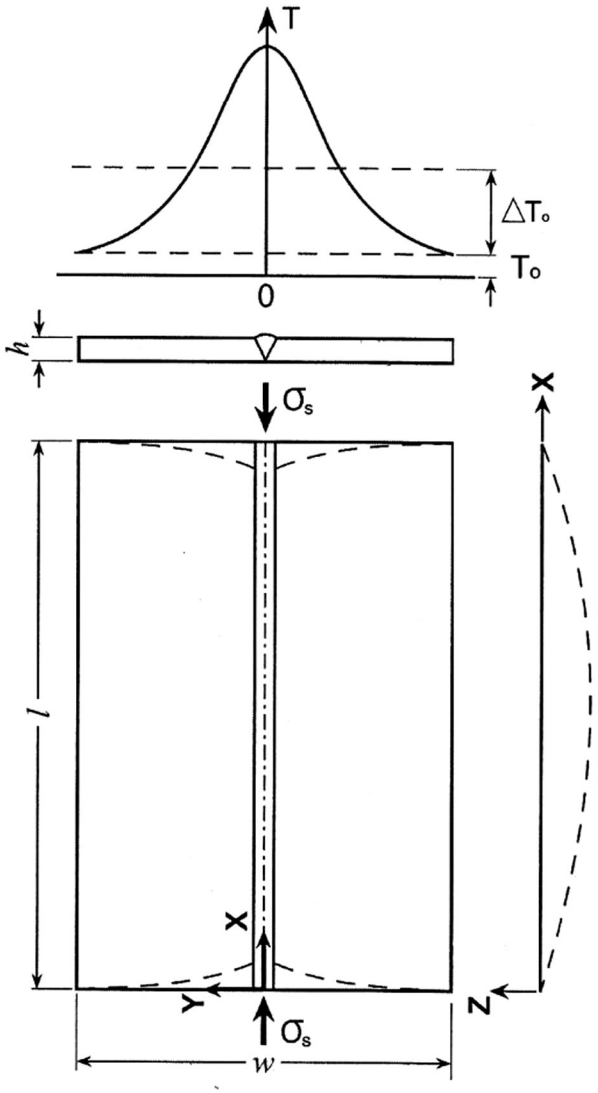

Fig. 7. Mechanism of buckling distortion in as welded condition.

The present investigation has shown that the STT technique is proved to be effective for minimisation of distortion and hence residual stress. However, the use of simultaneous cooling and heating during STT treatment could influence weld microstructure and mechanical properties and these are discussed in the next sections.

3.3. Weld metal microstructures

Fig. 8 shows weld metal microstructures under STT-treatments. All microstructures are composed of dendritic structures of α-phase (light-etched) with β-phases (dark-etched) were precipitated within dendritic arm spacings. It seems that STT treatment changes weld metal microstructures due to different weld cooling rates. From the view point of microstructure analysis, the effect of quenching induced by the cooling system is to accelerate the weld cooling rate resulting in finer microstructure (Fig. 8b) compared to that present in the conventional weld metal (Fig. 8a). However, this effect tends to diminish as the heating temperature is further increased to 200 and 300 °C resulting in lower cooling rates. As a result, coarse microstructures are formed as shown in Fig. 8c–d.

3.4. Hardness distributions

Hardness distributions along weld metal (WM), heat affected zone (HAZ) and base metal (BM) are shown in Fig. 9. Among these regions, the HAZ region has relatively higher values of hardness for all weld specimens, probably due to precipitation of β-phases during welding process whereas the weld metal region seems to have the lowest hardness.

In all weld joints under study, the highest weld metal hardness is observed in the STT treated weld joint with the heating temperature of 100 °C owing to a high cooling rate which promotes fine-grained microstructure.

3.5. Tensile stresses

Fig. 10 shows tensile test results for all welds under study. The ultimate stress or strength of the base metal is higher than that of weld specimens and therefore, fracture occurred at the weld region. It can be seen that the STT-treated weld with the heating temperature of 100 °C has the highest strength. This result is consistent with its microstructure and hardness. It has been known that faster cooling rate produces finer grained microstructure hence increasing strength

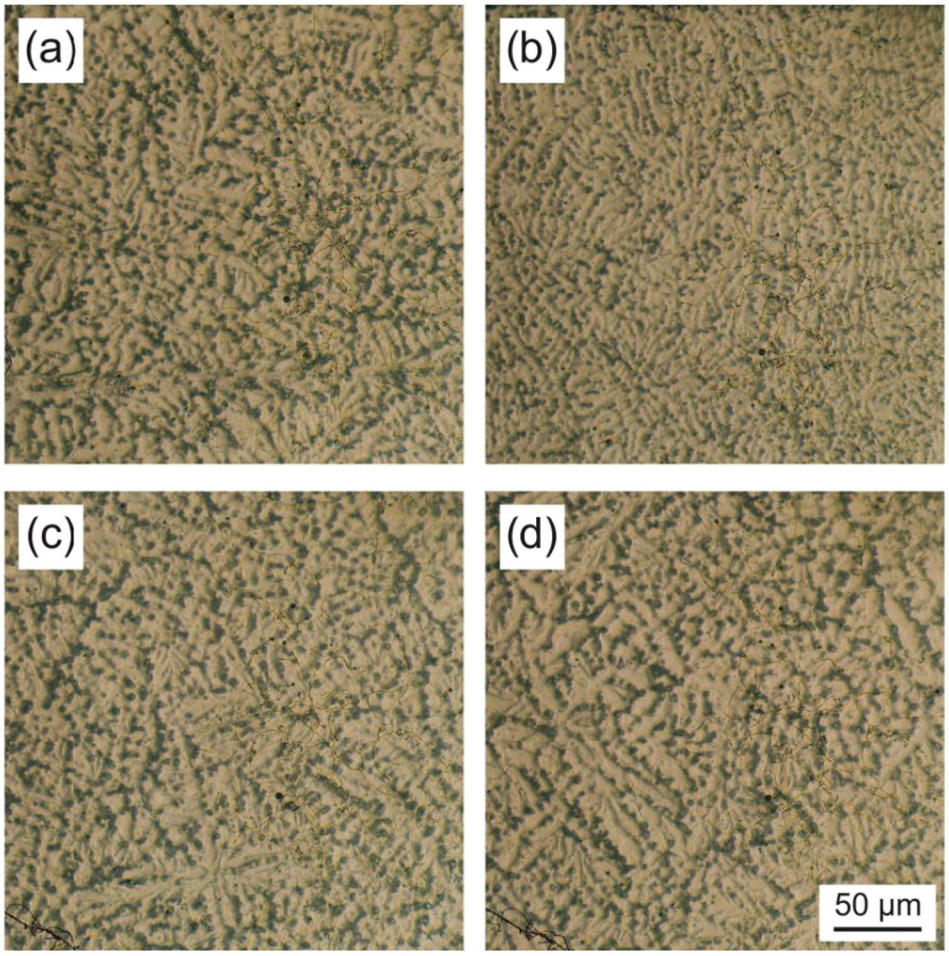

Fig. 8. Weld metal microstructures in (a) as welded condition and (b), (c), (d): the STT treated welds with heating temperatures of 100 °C, 200 °C and 300 °C respectively.

of weld joints according to Hall-Petch relationship. In addition, for most metals, tensile strength is linearly proportional to hardness since both properties are indicators of a metal's resistance to plastic deformation [35]. The yield stresses for all samples are around 0.7 to 0.8% of their strengths.

Considering the results of tensile test, examination of microstructure and hardness measurement, it is concluded that the minimum distortion of welded plate resulted from a STT treatment is not always accompanied by maximum static properties.

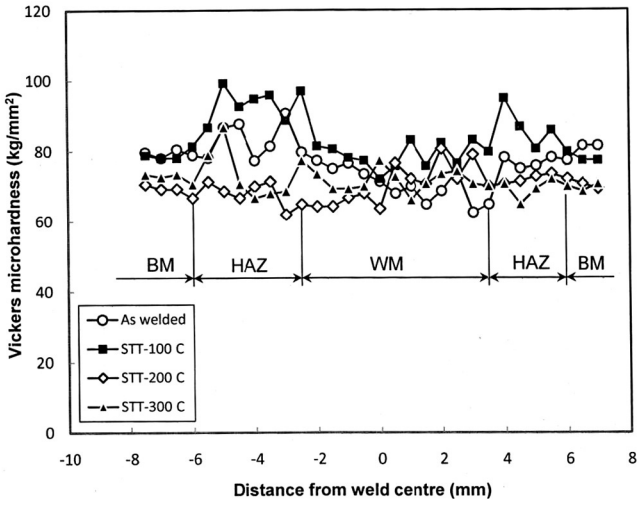

Fig. 9. Hardness distributions of 5083 aluminium alloy MIG welded joints under various STT treatments.

3.6. Residual stresses

Residual stress studies in this paper are focused on the weld which produces minimum out of plane distortion, i.e. the weld treated with STT at the heating temperature of 200 °C and as a comparison, the weld prepared in as welded condition is also used. Longitudinal residual strain and stress distributions for both the welded plates are shown in Fig. 11. Of note is that the accuracy of strain measurements in the present investigation is of the order of 10^{-4} resulting in a resolution in residual stress of ± 20 MPa. In Fig. 11a, residual strains in as welded condition are positive at the weld centre line and its adjacent area forming strain plateau then the strains become negative at the distance of 30 mm or more from the weld centre line. The effect of STT at heating temperature of 200 °C seems to shift the strain distribution to the more negative values. Subsequently, the strain measurement results can be used to calculate weld residual stresses as shown in Fig. 11b. It can be seen that residual stress profile in as welded condition is marked by tensile residual stress peaks at the weld region and its adjacent area followed by a decrease in the residual stress as the distance moves away from the weld centre line. The maximum value of residual stress is observed at HAZ, approximately 150 MPa that is slightly below its yield stress. The effect of STT treatment with heating temperature of 200 °C is to reduce the tensile residual stress at the weld centreline resulting in compressive residual stresses.

The distribution of transverse residual strain and stress at the middle of the welded plate length along transverse (y-direction) is

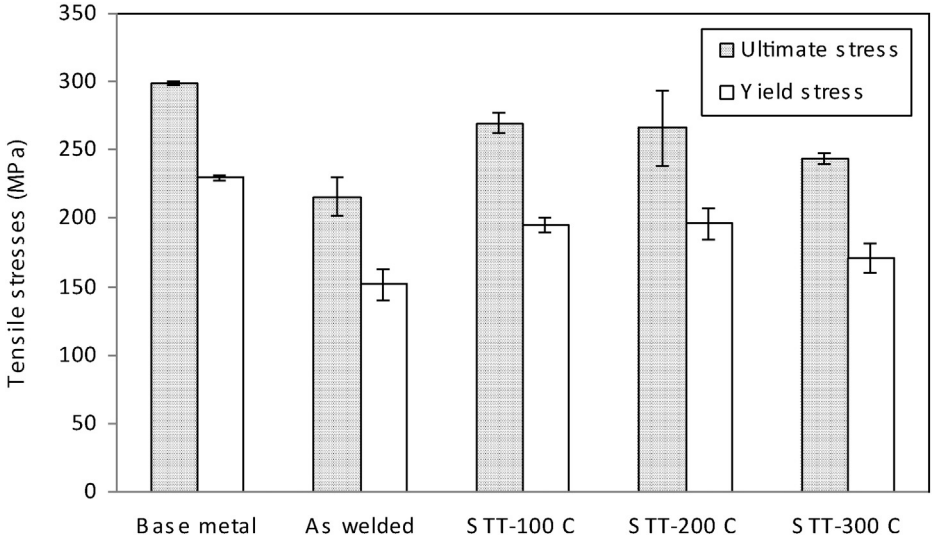

Fig. 10. Tensile stresses of 5083 aluminium alloy MIG weld metals.

shown in Fig. 12. Transverse residual strain profile in Fig. 12a is marked by a minimum positive strain, typically 54 μ (5.4×10^{-5}) at the weld centre line and then the strain is relatively constant up to the distance of 45 mm from the weld centre line. The STT treatment at a temperature of 200 °C causes the strain in the weld zone to become negative with the magnitude of 1900 μ (1.9×10^{-3}). The corresponding residual stresses obtained from the strain measurements are shown in Fig. 12b. It can be seen that the width of tensile residual stress profile in as welded condition is considerably large with the peaks of around 100 MPa. The STT treatment seems to reduce the transverse residual stresses resulting in compressive residual stresses in the weld zone.

It is worth noting that tensile transverse residual stresses are lower than tensile longitudinal residual stresses for both as welded and STT-treated welded plates. These results seem to suggest that expansion and contraction/shrinkage during welding along a weld centreline are much higher than perpendicular to the weld giving buckling is the dominant distortion in all AA5083 welded plates.

Of note is that both longitudinal and transverse residual stresses in the as welded condition appear to be in non-equilibrium condition

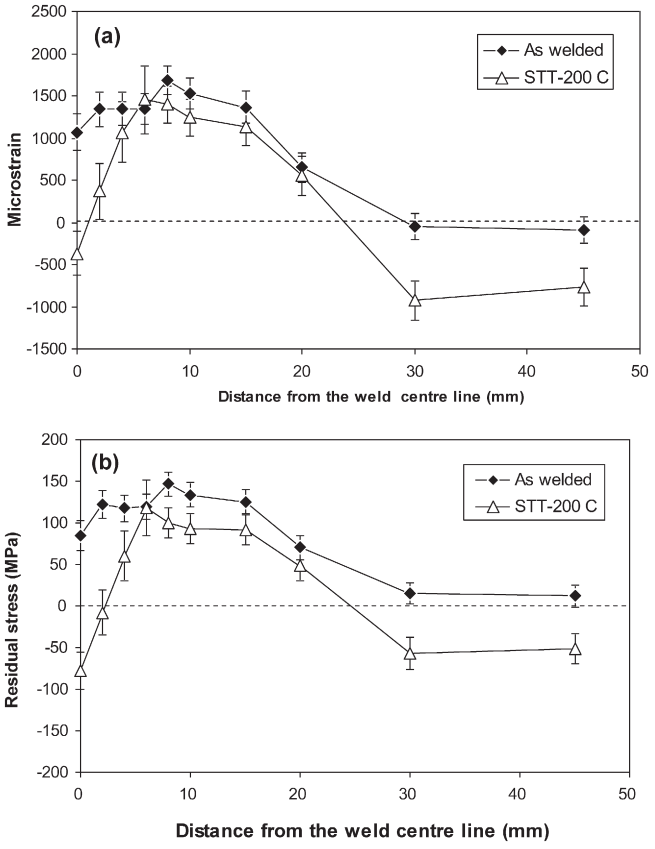

Fig. 11. The distribution of longitudinal residual: (a) strain and (b) stress in as welded and STT-200 °C treated conditions.

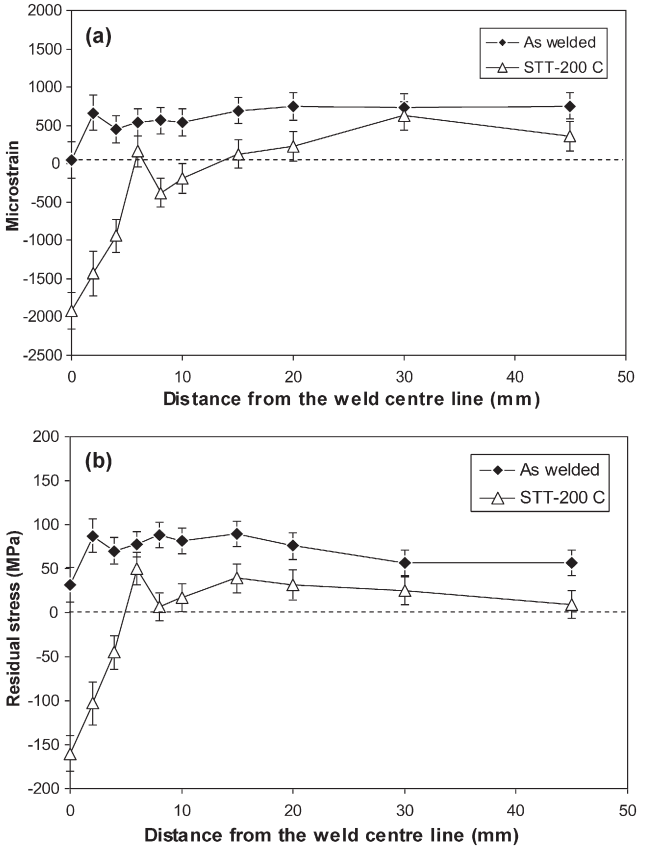

Fig. 12. The distribution of transverse residual: (a) strain and (b) stress in as welded and STT-200 °C treated conditions.

that is different to that commonly observed in 'normal' weld residual stresses. It may be argued that despite the residual stresses of the as welded plate are not yet in equilibrium, even tensile residual stresses still exists at the distance of 45 mm from the weld centreline, but they are probably balanced by 'reaction' stresses at the plate ends or other regions. Another possible explanation is that thermal stresses arise in the buckled welded plate during welding cause excessive plastic deformation or distortion. From atomic perspective, this distortion corresponds to an increase in *d*-spacings. It seems probably that in the buckled specimens which have relatively high *d*-spacings, the residual stresses obtained using *d*-spacing measurements (Eq. (5)) are shifted to more positive stress values.

3.7. Fatigue crack growth behaviours

Fig. 13 shows fatigue crack growth rate (FCGR) behaviours of welded joints in as welded condition and STT condition with the heating temperature of 200 °C. It can be seen that the fatigue crack growth curves exhibit three distinct regions, namely regions I, II and III. FCGRs in stable crack growth region, i.e. region II for both weld specimens are linear and they seem to follow Paris law as given by:

$$da/dN = C(\Delta K)^n \tag{14}$$

where da/dN is FCGR whereas ΔK is stress intensity factor range which is the difference between maximum and minimum stress intensity factors, (K_{max}–K_{min}) during the load cycle. By taking trendlines in the regions II then C and n which are known as Paris constants can be determined and the results are given in Table 3. The lower values of C and n obtained in the STT-treated weld suggest that STT method improves the weld fatigue performance. Another parameter which influences fatigue crack growth behaviour is minimum to maximum load ratio, R ($R = K_{min}/K_{max}$). Despite region II is not sensitive to R but an increase in R can move the regions I and III to lower ΔK values.

The retardation of da/dN in this investigation could be linked to transverse residual stresses which act parallel to dynamic applied stress direction. The interactions between residual stress and fatigue crack growth are complex where the magnitude and distribution of residual stresses change as the crack propagates. Despite Fig. 12 does not provide complete information with regard to the distribution of transverse residual stresses along the length of the weld (x-axis) but based on this figure, it can be predicted that in as welded condition, tensile transverse residual stresses are likely to form in the middle part of the welded plate length along x-axis and these stresses are balanced by compressive residual stresses at both ends of the plate as shown in Fig. 14. The STT treatment seems to change the magnitude and distribution of the residual stresses with the tensile transverse residual stresses formerly present in the middle part of the welded plate being replaced by compressive transverse residual stresses. Of note is that the dotted lines in Fig. 14 represent the magnitude of residual stresses before the initial crack was made.

Table 3
Paris constants.

Weld joints	C	n
As welded	5.6322E-11	3.5640
STT-200 °C	3.8222E-11	3.4978

If this assumption is operative then based on superposition approach [36,37], the retardation of FCGR could be linked to compressive residual stresses. The compressive residual stresses resulted from STT treatment, if they are superimposed on the dynamic applied stresses, reduce overall mean stress hence lowering fatigue crack growth rate. Further explanations of residual stress effect on fatigue crack growth of MIG aluminium alloy 5083 welds are suggested as follows. The presence of residual stresses changes the nominal stress intensity factors (K) and the stress ratio (R) to:

$$\Delta K_{eff} = (K_{\max} + K_{res}) - (K_{\min} + K_{res}) \tag{15}$$

$$R_{eff} = \frac{K_{\min} + K_{res}}{K_{\max} + K_{res}} \tag{16}$$

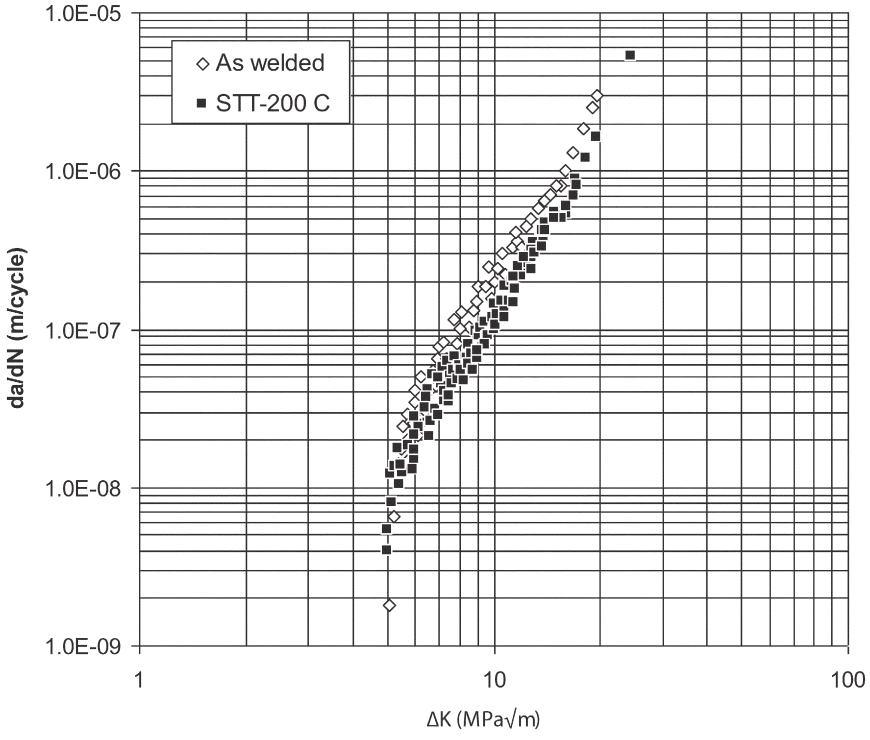

Fig. 13. Fatigue crack growth rates of as welded and STT-treated weld metals.

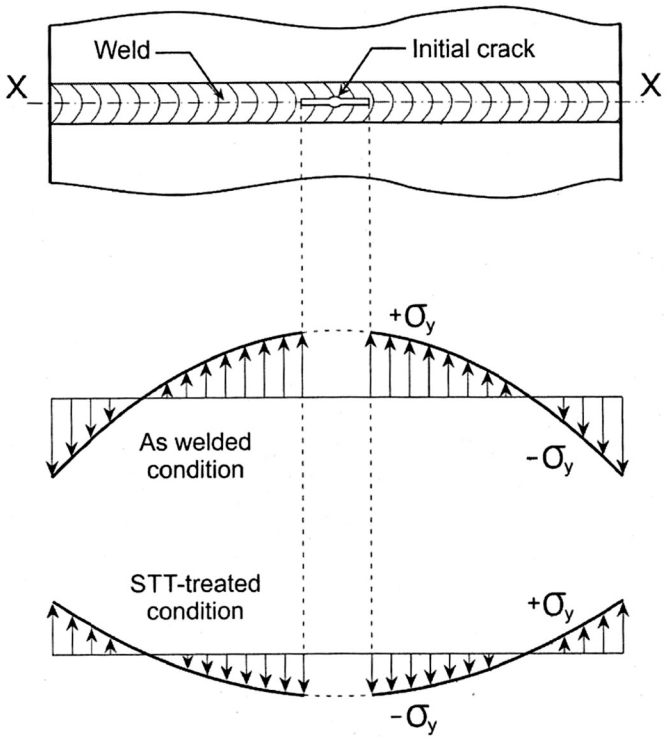

Fig. 14. A model for transverse residual stresses along the weldline for as welded and STT-treated weld joints.

where ΔK_{eff} is effective stress intensity factor range, K_{res} is the stress intensity factor due to residual stress and R_{eff} is stress ratio by considering residual stresses. The effects of residual stresses can be accounted for by considering Eqs. (15) and (16). The presence of tensile residual stress causes K_{res} to become positive hence increasing R_{eff} whilst ΔK_{eff} remains constant, i.e. $\Delta K_{eff} = \Delta K$. This means that the presence of tensile residual stress decreases crack closure and the crack remains open during cyclic loading due to high R_{eff}. In contrast, compressive residual stresses produce negative K_{res} hence decreasing R_{eff}. Furthermore, if $|K_{res}| \geq K_{\min}$ then the term of $(K_{min} + K_{res})$ in Eq. (15) would be zero since it does not contribute to fatigue crack growth so that ΔK_{eff} is reduced to:

$$\Delta K_{eff} = K_{\max} + K_{res} - 0 = K_{\max} + K_{res}. \tag{17}$$

In such a case as this, the Paris law (Eq. (10)) is modified as given by:

$$da/dN = C(\Delta K_{eff})^n. \tag{18}$$

Referring to Eq. (18), it can be concluded that compressive residual stress, if its stress intensity factor, K_{res} is higher than K_{min}, will reduce ΔK resulting in closure and hence low fatigue crack growth rate.

Results of SEM fractography study as shown in Figs. 15 and 16 seem to support this argument. Fig. 15 shows that large striations, typically more than 10 μm form on fracture surface of as welded weld metal with the crack direction from left to right. In STT-treated condition (Fig. 16), very clear striations with finer striation spacings are observed due to low ΔK_{eff}. Another feature seen in the SEM fractograph is the presence of smearing indicative of crack closure as the result of contact between crack surfaces.

Buckling and angular distortions as observed in the centre crack tension (CCT) specimens of as welded welds could contribute to deteriorating influence on fatigue crack growth behaviour due to additional bending stress. During experiment, both the CCT-specimen ends were clamped and in such fixed-fixed ends, stresses acting on the buckled specimen are shown in Fig. 17.

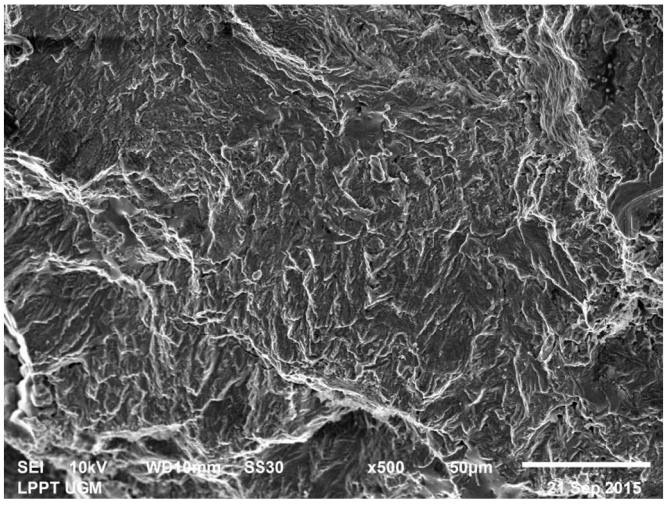

Fig. 15. Fracture surface of as welded weld metal.

Due to buckling distortion, the reaction force at any location x to balance an applied axial load P is shifted from the neutral axis to the distance of y resulting in bending according to:

$$M_x = M_a + Py \tag{19}$$

where M_a is fixed end moment. Accordingly, the bending stress at point x is governed by the equation:

$$\sigma_b = \pm \frac{M_x . z_c}{I_z} = \pm \frac{M_x (h/2)}{wh^3/12} = \pm \frac{6M_x}{wh^2}. \tag{20}$$

Based on superposition approach, the overall stress acting on buckled CCT-specimens is determined as:

$$\sigma_T = \sigma_{app} \pm \sigma_{res} \pm \sigma_b \tag{21}$$

where σ_{app}, σ_{res} and σ_b are applied axial stress, residual stress and bending stress respectively. Referring to Eqs. (19) and (20), the maximum bending moment and also bending stress occur at the middle span $(x = L/2)$ at which the initial crack (a_o) was located. This makes stresses at the crack tip to become more complex.

The present investigation has endeavoured to comprehensively study static thermal tensioning for minimisation of distortion and

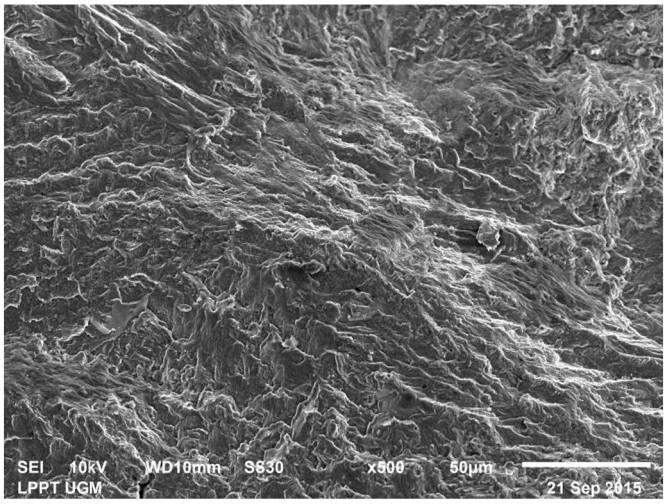

Fig. 16. Fracture surfaces of STT-treated weld metal.

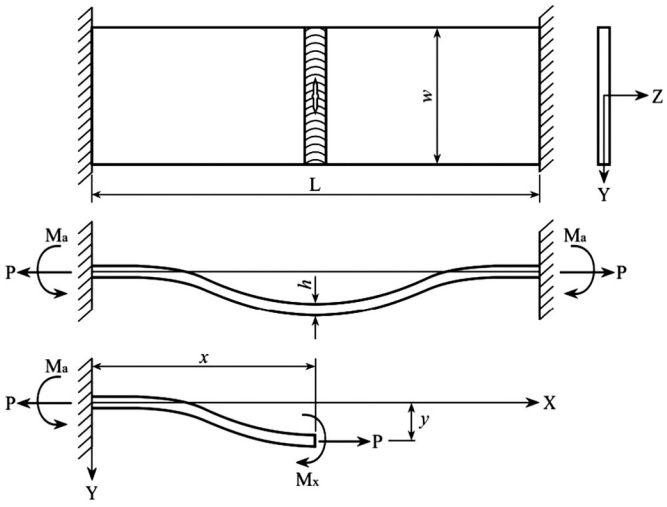

Fig. 17. A modelling of fixed-end forces of a buckled thin CCT-specimen.

residual stress by considering its effects on microstructure, mechanical properties and fatigue performance. Further work on fatigue crack growth rates by considering distortion needs to be carried out using experimental and modelling approaches to complement this work.

4. Conclusions

The conclusions that can be drawn from this investigation are summarised as follows:

Out of plane distortion can be reduced by stretching effect generated by static thermal tensioning (STT) treatment which counterbalances the distortion induced by welding.

The use of simultaneous cooling and heating during STT treatment modifies weld thermal cycle which affects weld microstructure and static properties such as hardness and strength.

Apart from control of distortion, STT treatment can reduce tensile residual stress and to a certain extent, compressive residual stress is formed.

It seems that retardation of fatigue crack propagation in STT-treated weld is associated with compressive residual stress induced by STT.

Acknowledgement

This work was conducted under research grant, named STRANAS with contract number: 025/SP2H/PL/Dit.Litabmas/II/2015. The authors acknowledge funding of DIKTI and Gadjah Mada University.

References

[1] R.L. Holtz, P.S. Pao, R.A. Bayles, T.M. Longazel, R. Goswami, Corrosion-fatigue behavior of aluminum alloy 5083-H131 sensitized at 448 K (175 °C), Metall. Mater. Trans. A 43A (2012) 2839–2849.
[2] J.C. Dutra, R.H.G. Silva, B.M. Savi, Metallurgical characterization of the 5083H116 aluminium alloy welded with the cold metal transfer process and two different wire-electrodes (5183 and 5087), Weld. World 59 (6) (2015) 797–807.
[3] P.M.G.P. Moreira, M.A.V. de Figueiredo, P.M.S.T. de Castro, Fatigue behaviour of FSW and MIG weldments for two aluminium alloys, Theor. Appl. Fract. Mech. 48 (2007) 169–177.
[4] D. Deng, Y. Zhou, T. Bi, X. Liu, Experimental and numerical investigations of welding distortion induced by CO_2 gas arc welding in thin-plate bead on joints, Mater. Des. 52 (2013) 720–729.
[5] D. Rosenthal, Mathematical theory of heat distribution during welding and cutting, Welding J. 20 (5) (1945) 220s–234s.
[6] N.N. Rykalin, Calculations of Thermal Processes in Welding, Mashgiz, Moscow, 1951.
[7] D. Radaj, Heat Effects of Welding: Temperature Field, Residual Stress, Distortion, Springer-Verlag, Berlin, 1992.
[8] P. Michaleris, Uncertainty quantification in modelling welding residual stress and distortion, Sci. Technol. Weld. Join. 16 (8) (2011) 722–727.
[9] M. Peric, Z. Tonkovic, A. Rodic, M. Surjak, I. Garasic, I. Boras, Numerical analysis and experimental investigation of welding residual stresses and distortions in a T-joint fillet weld, Mater. Des. 53 (2014) 1052–1063.
[10] J. Sun, X. Liu, Y. Tong, D. Deng, A comparative study on welding temperature fields, residual stress distributions and deformations induced by laser beam welding and CO_2 gas arc welding, Mater. Des. 63 (2014) 519–530.
[11] Y.P. Yang, R. Dull, H. Castner, T.D. Huang, D. Fanguy, Material strength effect on weld shrinkage and distortion, Weld. J. 93 (2014) 421–430.
[12] Y. Ueda, H. Murakawa, Ma N, Welding Deformation and Residual Stress Prevention, Butterworth-Heinemann, Oxford, 2012.
[13] T. Gray, D. Camilleri, N. McPherson, Control of Welding Distortion in Thin-Plate Fabrication, Woodhead Publishing Ltd., Cambridge, UK, 2014.
[14] F.W. Brust, D.S. Kim, Mitigating welding residual stress and distortion, in: Z. Feng (Ed.), Processes and mechanisms of welding residual stress and distortion, Woodhead Publishing Ltd., Cambridge, England 2005, pp. 264–294.
[15] P. Michaleris, Minimization of Welding Distortion and Buckling: Modelling and Implementation, Woodhead Publishing Ltd., Cambridge, England, 2011.
[16] M. Mochizuki, M. Toyoda, Weld distortion control during welding process with reverse-side heating, ASME J. Pressure Vessel Tech. 129 (2007) 619–629.
[17] Yal Burak, L.P. Bisijina, YaP Romanjuk, A.A. Kazimirov, V.P. Morgun, Controlling the longitudinal plastic shrinkage of metal during welding, Avtom. Svarka 288 (3) (1977) 27–29.
[18] Yal Burak, YaP Romanjuk, A.A. Kazimirov, V.P. Morgun, Selection of the optimum fields for preheating plates before welding, Avtom. Svarka 314 (5) (1979) 5–9.
[19] P. Michaleris, X. Sun, Finite element analysis of thermal tensioning techniques mitigating weld buckling distortion, Weld. J. 76 (22) (1997) 451–457.
[20] S. Guo, X. Li, Welding control of thin Al alloy plate by static thermal tensioning, J. Mater. Sci. Technol. 17 (1) (2001) 163–164.
[21] M.V. Deo, P. Michaleris, Mitigation of welding-induced buckling distortion using transient thermal tensioning, Sci. Technol. Weld. Join. 8 (1) (2003) 49–53.
[22] P. Michaleris, J.A. Dantzig, D.A. Tortorelli, Minimization of welding residual stress and distortion in large structures, Weld. J. 78 (11) (1999) 361–366.
[23] J. Song, J. Shanghvi, P. Michaleris, Optimization of thermo-elasto-plastic manufacturing processes, Comput. Meth. in Appl. Mech. Eng. 193 (2004) 4541–4566.
[24] Guan Q. Control of buckling distortions in plates and shells. In: Feng Z. Ed. Processes and mechanisms of welding residual stress and distortion. Cambridge, England: Woodhead Publishing Ltd.;2005: 295–343.
[25] J. Li, Localized thermal tensioning technique to prevent buckling distortion, Weld. World 49 (11/12) (2005) 4–14.
[26] Li J, Shi QY. Minimizing buckling distortion in welding by weld cooling. In: Michaleris Ed. Minimization of welding distortion and buckling: modelling and implementation. Cambridge, England: Woodhead Publishing Ltd.;2011:214–72.
[27] C. Jang, P.Y. Cho, M. Kim, S.J. Oh, J.S. Yang, Effects of microstructure and residual stress on fatigue crack growth of stainless steel narrow gap welds, Mater. Des. 31 (4) (2010) 1862–1870.
[28] Y.E. Ma, P. Staron, T. Fischer, P.E. Irving, Size effects on residual stress and fatigue crack growth in friction stir welded 2195-T8 aluminium-part I: experiments, Int. J. Fatigue 33 (2011) 1417–1425.
[29] C.D.M. Liljedahl, O. Zanellato, M.E. Fitzpatrick, J. Lin, L. Erwards, The effect of weld residual stresses and their re-distribution with crack growth during fatigue under constant amplitude loading, Int. J. Fatigue 32 (2010) 735–743.
[30] G.A. Webster, R.C. Wimpory, Non-destructive measurement of residual stress by neutron diffraction, J. Mater. Process. Technol. 117 (2001) 395–399.
[31] D.B. Darmadi, A.K. Tieu, J. Norrish, A validated thermal model of bead-on-plate welding, Heat Mass Transf. 48 (2012) 1219–1230.
[32] Y. Guo, D. Wu, G. Ma, D. Guo, Trailing heat sink effects on residual stress and distortion of pulsed laser welded Hastelloy C-276 thin sheets, J. Mater. Process. Technol. 214 (2014) 2891–2899.
[33] Y.P. Yang, P. Dong, Buckling distortion and mitigation techniques for thin-section structures, J. Mater. Eng. Perform. 21 (2) (2012) 153–160.
[34] M.N. Ilman, Iswanto Kusmono, Fatigue crack growth rate behaviour of friction-stir aluminium alloy AA2024-T3 welds under transient thermal tensioning, Mater. Des. 50 (2013) 235–243.
[35] W.D. Callister, Materials Science and Engineering, fourth ed. John Willey & Sons. Inc., New York, 1997.
[36] Y.E. Ma, P. Staron, T. Fischer, P.E. Irving, Size effects on residual stress and fatigue crack growth in friction stir welded 2195-T8 aluminium-part II: modelling, Int. J. Fatigue 33 (2011) 1426–1434.
[37] C.J. Lammi, D.A. Lados, Effects of processing residual stresses on fatigue crack growth behavior of structural materials: Experimental approachess and microstructural mechanisms, Metall. Mater. Trans. A 43A (2012) 87–107.